

# Concentration-dependent viscous mixing in microfluidics: modelings and experiments

Chaoqun Wu<sup>1</sup> · Kai Tang<sup>1</sup> · Bing Gu<sup>2</sup> · Jie Deng<sup>3</sup> · Zhenhua Liu<sup>3</sup> · Zhigang Wu<sup>3</sup>

Received: 4 January 2016 / Accepted: 19 May 2016 / Published online: 31 May 2016  
© Springer-Verlag Berlin Heidelberg 2016

**Abstract** In microfluidic mixing, great attention has been devoted to the structural design to enhance mixing efficiency. However, the influence of the variant viscosity in the mixing process is rarely discussed due to the practical challenges originated from the strong and complex couplings between species concentration and other fluid properties such as density, viscosity and diffusion coefficient. In this work, a group of coupling relationships among concentration, density, viscosity, as well as diffusion coefficient are introduced to accurately simulate the mixing process with a viscous flow involved. Compared with the traditional linear approximation, the new approach is more suitable to simulate the concentration-dependent viscous mixing in microfluidics. Furthermore, a planar passive micromixer is designed to validate the coupling approach from both modeling and experiment perspectives. By comparing experimental and numerical results, it turns out that the coupling approach achieves higher accuracy than the traditional linear approximation. In addition, four derived models are experimentally tested and numerically simulated by adopting the new method. The results of each model reach a good agreement between modeling and experiment.

**Keywords** Concentration-dependent · Viscous mixing · Fluid properties · Passive micromixer · Chaotic advection

## 1 Introduction

Driven by micrototal analysis systems ( $\mu$ TAS) (Auroux et al. 2002; Patabadige et al. 2016; Reyes et al. 2002) or so-called lab-on-a-chip (LoC) technologies in the applications (Jeong et al. 2010; Sackmann et al. 2014) of sample preparation and analysis, chemical synthesis, drug discovery, as well as DNA sequencing, micromixers have attracted great interests from both the research community and commercial sector all over the world. Being considered as one of the most essential processes among such miniaturized systems, mixing of fluids offers significant advantages of low reagent consumption and rapid response for biochemical analysis. Nevertheless, fluid mixing in such conditions is a great challenge due to a strict laminar flow regime, which means the mixing process is dominated by molecular diffusion. This slow mixing mechanism generally demands extended channel and intricate structure and thus negates many of the advantages of miniaturization. In the past few decades, numerous efforts have been made to solve this annoying conundrum and meet the mixing requirement in various applications (Nguyen and Wu 2005; Ward and Fan 2015).

In most of the previous work, fluid properties are regarded as constant. The change of fluid parameter (such as viscosity) induced by mixing process is seldom taken into account. However, when mixing two types of fluids with large difference in viscous, the mixed fluid leads to a changed concentration and viscosity and hence the changed diffusion coefficient, which exerts significant impact on the original flow field distribution (such as velocity gradient)

---

Chaoqun Wu, Kai Tang and Bing Gu contributed equally to this work.

---

✉ Zhigang Wu  
zgwu@hust.edu.cn

- <sup>1</sup> School of Mechanical and Electronic Engineering, Wuhan University of Technology, Wuhan 430070, China
- <sup>2</sup> Chinese PLA General Hospital, Beijing 100853, China
- <sup>3</sup> State Key Laboratory of Digital Manufacturing and Equipment Technology, School of Mechanical Science and Engineering, Huazhong University of Science and Technology, Wuhan 430074, China

and further the species distribution. The omission of these strong concentration-dependent coupling relationships will lead to significant errors when fluids with noticeable viscous difference are to be mixed. In the traditional method, only the physical parameters of solvent, e.g., density and viscosity, have been taken into consideration as that in Cook et al. (2013), or simply set the properties of two types of working fluids as constant separately and then obtained species distributions through solving their respective convection–diffusion equation (Alam et al. 2014). In the above work, diffusion coefficient was also set to be a constant, which may cause imprecise results and tremendous errors when a fluid with high viscosity is involved. In order to achieve high-precision concentration prediction, it becomes necessary to include the concentration-dependent fluid properties, e.g., density, viscosity and corresponding diffusion constant, into the entire modeling process.

Taking great advantages from transverse flow to stretch, fold and breakup streams to enhance mixing, the researches on chaotic advection-based micromixers have been a hot-spot for many years (Lee et al. 2016). In such kind of studies, various microstructures such as curved (Solehati et al. 2014; Yamaguchi et al. 2004), zigzag, square wave (Kuo and Jiang 2014), circular mixing chamber (Ansari and Kim 2009) and converging–diverging structure (Cheri et al. 2013) have been proposed to form vortex to accelerate species transport. According to Hessel et al. (2005), the next development of micromixers should focus on the improvement of the existing structures. Thus, various multi-feature micromixers (Sudarsan and Ugaz 2006; Wu and Tsai 2013) have been proposed through combining different disturbance effects to further enhance the mixing.

Introducing a group of coupling formulas among species concentration, viscosity, as well as diffusion coefficient into the flow equations, this work aims at accurately studying the mixing process from both modeling and experiment perspectives. A series of studies on passive micromixer equipped with multi-feature structure including mixing units of non-coaxial rectangular chamber and curved channel as well as expansion chamber is conducted. A comparison between traditional linear approximation and the coupling method discussed in this paper is performed, and the latter shows a better accuracy.

## 2 Numerical modeling

Two types of working fluids, water and glycerol–water solution, are considered in the present modeling. In the microchannel, their properties are ever changing during the mixing process and can be described by the mass distribution. The mixture's density is directly derived from the proportion of each component and is predicted by:

$$\rho = \rho_g \omega + \rho_w (1 - \omega) \quad (1)$$

where  $\omega$  is the mass fraction of glycerol in mixture; the subscripts of  $g$  and  $w$  denote glycerol and water, respectively. According to Cheng (2008), the mixture's viscosity  $\mu$  is related to the two components in the form of nonlinear exponential function:

$$\mu = \mu_g \exp\left(\alpha \cdot \ln \frac{\mu_w}{\mu_g}\right) \quad (2)$$

where  $\alpha$  is the weighting factor of glycerol, which can be calculated by

$$\alpha = 1 - \omega + \frac{ab\omega(1 - \omega)}{a\omega + b(1 - \omega)} \quad (3)$$

where  $a$  and  $b$  are coefficients associated with the operation temperature. Diffusion coefficient of the mixture can be estimated by the Einstein–Stokes equation:

$$D = \frac{kT}{6\pi\mu R} \quad (4)$$

where  $k$  is the Boltzmann's constant,  $T$  is the absolute temperature (K), and  $R$  is the particle radius. According to the above equations, the mixture's density and viscosity depend on the local concentration, and the diffusion coefficient is inversely proportional to its local viscosity. The mixing process is normally simulated through solving Navier–Stokes equation and continuity equation, as well as convection–diffusion equation. By introducing Eqs. 1–4, fluid properties in these equations are turned into concentration dependent.

A planar passive micromixer was designed in the present research. The schematic diagram of the proposed micromixer is shown in Fig. 1a. Special mixing features of non-coaxial rectangular chamber, curved channel and expansion chamber are included in this design. The height ( $H$ ) and width ( $W_1$ ) of the inlets were designed to be 60 and 90  $\mu\text{m}$ , respectively. A fillet is placed at the confluence of the cruciform inlet structure with the radius  $R_2$  of 0.05 mm. The length of the straight channel after confluence  $L_1$  is 1 mm. The length of the non-coaxial rectangular chamber  $L_2$  is 0.8 mm. The ratio of  $W_2/W_1$  equals to 8 (named model A hereinafter). The outer curvature radius of the curved channel  $R_1$  is designed to be 0.6 mm, and the cross section of this part is  $90 \times 60 \mu\text{m}$  ( $W_1 \times H$ ). To avoid sagging, the expansion ratio of the expansion chamber ( $W_3/W_1$ ) is assigned as 5. Disturbance resulted from inlets and outlet has a great effect on the flow state at this region. Therefore, in order to keep experiment results free from these confounding factors, the lengths of inlets and outlet are set as 10 times of the width of the corresponding channel.

Numerical simulations were performed on this micromixer by using the commercial program of COMSOL

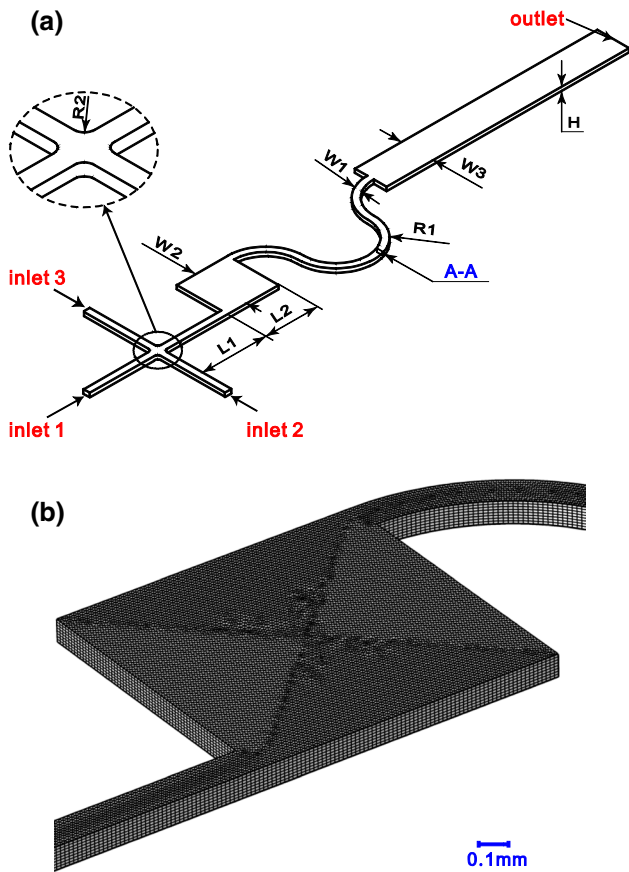


**Fig. 1** Schematic diagrams of the micromixer designed in the simulation: **a** structural layout and geometric parameters, and **b** the grid system used in the numerical simulation. The cross section of A–A is positioned in the middle of the curved channel

Multiphysics 5.1 based on finite element method (FEM). Physical models in terms of laminar flow and transport of diluted species were employed in the simulation. The flow regime was considered to be viscous, incompressible and isothermal in a steady state. The properties of water and glycerol taken at room temperature (25 °C) are listed in Table 1. On account of the viscosity of the blood is around 4 times of the water, 45.5 % glycerol–water solution (with the similar viscosity of human blood) was selected as the high viscous working fluid. The coefficients of *a* and *b* in Eq. 3 are equal to 0.6625 and 2.072, respectively, under this circumstance. In the flow field, initial values of velocity and concentration were set as default of 0 m/s in all directions and 0 mol/m<sup>3</sup>. Glycerol solution was assigned to inlet 1 and pure water to inlet 2 and 3 with the boundary condition of inlet velocity. The velocity in the inlet 2 and 3 was set as one-half of that in the inlet 1, which was performed for Reynolds number ( $Re = \rho uL/\mu$ , where  $\rho$  is the fluid density, *u* is the mean velocity, *L* is the characteristic length of inlet, and  $\mu$  denotes fluid viscosity) of water ranging from 0.1 to 200. This cruciform inlet structure is

**Table 1** Properties of fluids at 25 °C

Fluid	Density (kg m <sup>-3</sup> )	Viscosity (kg m <sup>-1</sup> s <sup>-1</sup> )
Water	996.85	$8.9274 \times 10^{-4}$
Glycerol	1260.65	0.90568

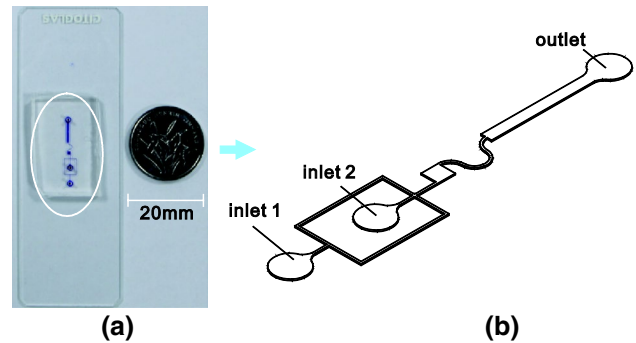


**Fig. 2** **a** Fabricated micromixer. **b** The designed structure of the micromixer

used to split the water into two streams, and then, both of them join and wrap the working flow coming from inlet 1 at the cruciform confluence. This structure can enlarge the contact area between these working fluids and significantly decrease the diffusion path. The mole concentration of glycerol was set to be 5518.3 mol/m<sup>3</sup> at inlet 1 and 0 mol/m<sup>3</sup> at other inlets. The boundary condition of the outlet was set to be pressure outlet with zero static pressure and outflow. Non-slip and no flux condition were applied at all of the solid walls.

This micromixer was meshed by triangular prism unstructured cells (see Fig. 1b). Additional boundary layers were also added at inlet 1 to avoid the possible numerical errors. Ultimately, ten thousand elements in all are included in the grid system. Moreover, high-order discretization was implemented to ensure the accuracy. As a consequence, about three million degrees of freedom were included in this numerical model. Navier–Stokes equation and convection–diffusion equation were stabilized by the generalized least squares (GLS) and the streamline upwind Petrov–Galerkin (SUPG) method, respectively, which reduced the numerical diffusion. These equations were solved via the solver of MUMPS (MULTifrontal Massively Parallel Sparse Direct Solver) in a full coupled way. That is, the obtained velocity through solving Navier–Stokes equation is used to calculate the concentration distribution in the convection–diffusion equation. Subsequently, the local concentration is used to calculate the local density and viscosity that impacts Navier–Stokes equation and the corresponding diffusion coefficient that impacts the convection–diffusion equation. All equations are iteratively solved by repeating

this procedure. The solutions are considered to have attained convergence for the relative error of less than 0.001.

To further optimize the mixing efficiency, the non-coaxial rectangular chamber was regarded as the optimization target and four derived models with different expansion ratios  $W_2/W_1$  of 1:1 (model B), 2:1 (model C), 4:1 (model D) and 16:1 (model E) were designed and tested.

### 3 Experimental methods

#### 3.1 Fabrication

A T-type structure was designed in inlet 1 to split the stream, as shown in Fig. 2. A standard soft lithography procedure (Xia and Whitesides 1998) was adopted to fabricate the molds of the micromixers. Firstly, moderate volume of SU-8 3050 (MicroChem Corp., USA) was dispensed on a cleaned silicon wafer and then spun by a spin coater to form a uniform layer with a thickness of 90  $\mu\text{m}$ . Subsequently, a prebake stage at 65  $^{\circ}\text{C}$  for 5 min took place and followed by a 20-min soft bake operation at 95  $^{\circ}\text{C}$ . After cooling down to the room temperature, the wafer was exposed to a UV light (HWUV225X, China) for 40 s that was equally divided into four times. Whereafter, a post-bake was operated at 65  $^{\circ}\text{C}$  for 1 min and 95  $^{\circ}\text{C}$  for 5 min. After cooling down, the wafer was bathed in 1-methoxy-2-propanol solvent (MicroChem Corp., USA) until the unexposed areas were washed off. The wafer was cleaned by isopropyl alcohol (Sinopharm Chemical Reagent Co. Ltd., China) and was dried by nitrogen, followed by a heating operation at 150  $^{\circ}\text{C}$  for 30 min in the oven. The wafer then received surface treatment with octyltrichlorosilane (Sigma-Aldrich, USA) by using a vacuum desiccator. A replica of this channel was formed by using polydimethylsiloxane (PDMS). Liquid PDMS (Elastosil RT601, Wacker, Germany), a 9:1 (mass/mass) mixture of silicone elastomer base and curing agent, was poured onto the wafer after removing the air bubbles. The mold then was heated in oven at 75  $^{\circ}\text{C}$  for 20 min. Afterward, the solid transparent PDMS was formed and was peeled off from the wafer. Pores of the inlets and outlet were punched with a blunt needle in the PDMS. At last, the PDMSs were irreversibly bonded with a glass slide through plasma treatment. Figure 2a presents the fabricated micromixer.

#### 3.2 Experimental setup

Figure 3 shows the experimental setup. To minimize systematic errors, a single multi-channel syringe pump (Fusion 100, Chemyx Inc., USA) was used to control the holistic flow rate ranging from 0.45–900  $\mu\text{l}/\text{min}$ , which corresponded to Re of water from 0.1 to 200. Two types of solutions of 45.5 % glycerol solution and deionized

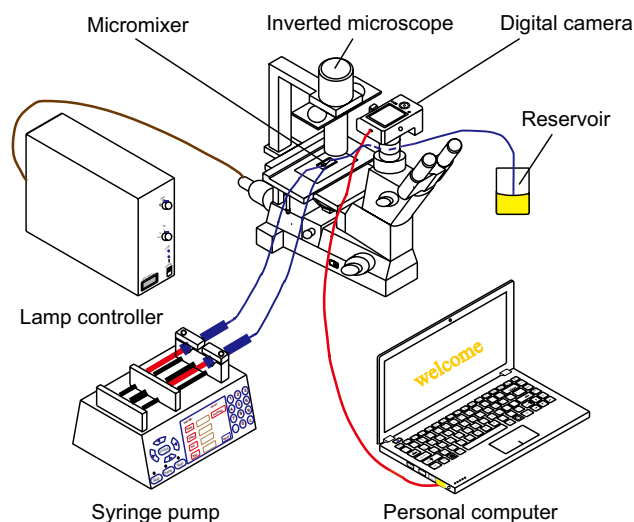


**Fig. 3** Experimental setup for flow visualization and image acquisition. Solutions are pumped into the micromixer by a multi-channel syringe pump, and the mixed liquid is collected by a reservoir. The inverted microscope with a lamp realizes the visualization of the mixing process, which is recorded by a digital camera remotely controlled by a personal computer

water labeled with fluorescence sodium (1.5 %) were prepared at the room temperature as the working fluids. During the operation process, water and glycerol solution were pumped into the microchannel through inlet 1 and inlet 2 (see Fig. 2b), respectively. An inverted microscope (ECLIPSE TS-100, Nikon, Japan) equipped with a halogen lamp realizes the visualization of microscale flow with magnification of 40. A computer-controlled high-resolution digital camera (EOS 70D, Canon, Japan) is mounted on the microscope to record the fluorescent images.

#### 3.3 Data acquisition

To make a quantitative analysis on mixing efficiency, an image processing operation with a MATLAB program (Wu et al. 2004) was performed. Firstly, the obtained images were cropped along edges of the microchannel. Secondly, the colors were converted into 8-bit grayscale images. The grayscale values in each pixel point at the outlet were normalized to values in the range of 0 to 1. Finally, the mixing index (M.I.) or mixing degree was quantified by calculating the standard deviation of the normalized grayscale value (between 0 and 1):

$$\gamma = \sqrt{\frac{1}{N} \sum_{i=1}^n (C_i - \bar{C}_m)^2} \quad (5)$$

$$M.I. = 1 - \sqrt{\frac{\gamma^2}{\gamma_{\max}^2}} \quad (6)$$

where  $C_i$  is local normalized grayscale value;  $i$  is the serial number of the sampling points;  $N$  is the total number of sampling points;  $\bar{C}_m$  is the average normalized grayscale value; and  $\gamma_{\max}$  is the maximum variance over the data range. Photographs taken at target zone (near the outlet but free from the outlet disturbance) are two-dimensional (from the top view), and flow is unstable at high flow rate. To eliminate random error, a plane with a dimension of  $0.5 \text{ mm} \times W_j$  at the target zone was extracted and calculated. The averaged value of M.I. was used to evaluate the mixing efficiency of the micromixer. The ultimate M.I. ranges from 0 to 1, where 1 and 0 denote completely mixed and completely unmixed, respectively. Equations 5 and 6 were also employed to evaluate the mixing efficiency in the modeling. The only difference is that  $C_i$  in Eq. 5 is the value of normalized concentration at the outlet.

### 4 Results and discussion

The linear approximation method discussed in the previous report (Wu and Nguyen 2005) is a method that the viscosity of the mixture is considered to be a linear function of the species volume fraction. The viscosity value is given by:

$$\eta = \eta_A \Phi_A + \eta_B \Phi_B \tag{7}$$

where  $\Phi_i$  denotes the species volume fraction and is derived by:

$$\Phi_i = c_i / c_{\max} \tag{8}$$

where  $c_i$  is the local concentration and  $c_{\max}$  is the maximum concentration of species  $i$ . With the consideration of strong coupling relationships existed in the mixing process, a nonlinear exponential function is introduced in this modeling work. A preliminary theoretical comparison between the two methods was performed to investigate their differences, as shown in Fig. 4. It can be found that viscosity values of linear approximation are larger than that of nonlinear approximation at normalized concentration from 0 to 1. Diffusion coefficient is inversely proportional to the viscosity according to the Einstein–Stokes equation. Consequently, diffusion coefficient curve of linear approximation is below the curve of nonlinear approximation. Linear approximation, by comparison, actually enlarges the effect of viscosity and weakens the effect of species diffusion at the same time, both of which underrate the mixing efficiency. As the normalized concentration increases, the slope of the viscosity curve derived from nonlinear approximation gradually increases. In contrast, viscosity curve of linear approximation keeps the constant rising slope. As can be seen in Fig. 4, the viscous difference between two

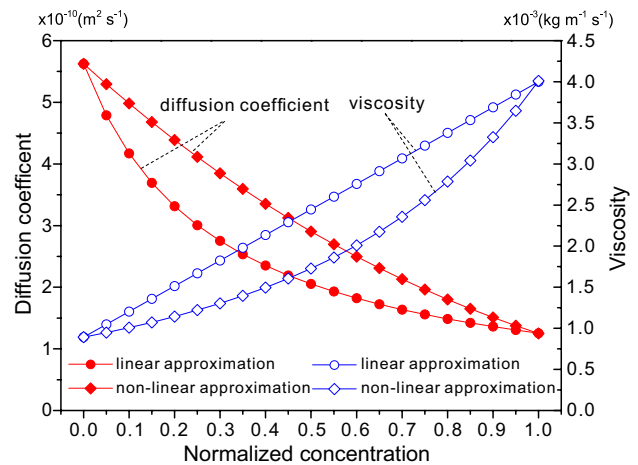


**Fig. 4** Comparison on the diffusion coefficient and viscosity resulted from linear approximation and nonlinear approximation, respectively. Linear approximation virtually enlarges the value of viscosity and contrarily decreases the value of diffusion coefficient

approaches reaches the maximum of 37.16 % when normalized concentration equals to 0.6.

To validate the coupling method, experiment and modeling including linear approximation and nonlinear approximation were performed on model A (see Fig. 1) with Re of water varying from 0.1 to 200. Figure 5 shows the distribution of different fluid parameters of concentration, viscosity and diffusion coefficient at Re = 25 and 200. For each method, the images on the left were taken from the mid-plane of the non-coaxial rectangular chamber and the images on the right were taken from the cross section of A–A in Fig. 1.

At low flow rate of Re = 25, inertial effect is too weak to induce strong disturbance; hence, the mass distribution keeps concentrated. It can be seen in Fig. 5a that the viscosity distribution is in conformity with the concentration distribution, but the diffusion coefficient distribution is on the exact opposite. The difference of mass distribution between linear approximation and nonlinear approximation mainly exists in the transition region. With the uniform rising gradient trait (referring to the viscosity curve of linear approximation in Fig. 4), the concentration and viscosity color nephograms derived from linear approximation method display a uniform change at the transition region, which makes it smooth from the perspective of visual (Fig. 5a). Compared with the linear approximation, the viscosity curve of nonlinear approximation shows smaller slope at low concentration section and bigger slope at high concentration section. Hence, the transition region shows fuzzy edges at low concentration area and clear edges at the high concentration area. In addition, there is a more intuitive phenomenon in the right pictures of Fig. 5a. The area occupied by glycerol solution (high concentration and high

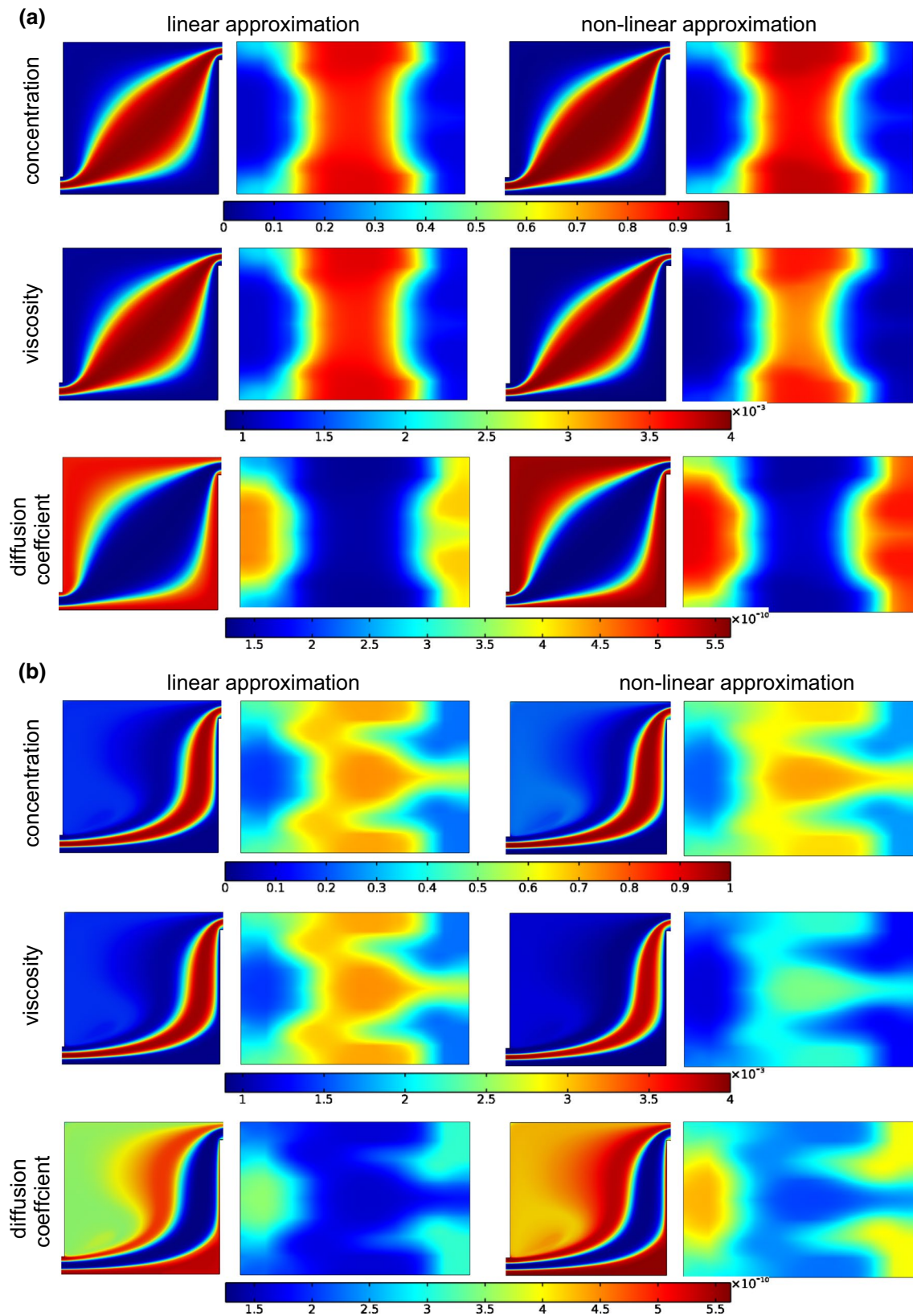


**Fig. 5** Comparison of the characteristics of fluid flow in terms of concentration distribution, viscosity distribution and diffusion coefficient distribution from simulations based on linear approximation and nonlinear approximation. The Reynolds number is **a**  $Re = 25$  and **b**

$Re = 200$ . For each method, the images on the *left* are taken from the mid-plane of the non-coaxial rectangular chamber, and the images on the *right* are taken from the cross section of A–A in Fig. 1

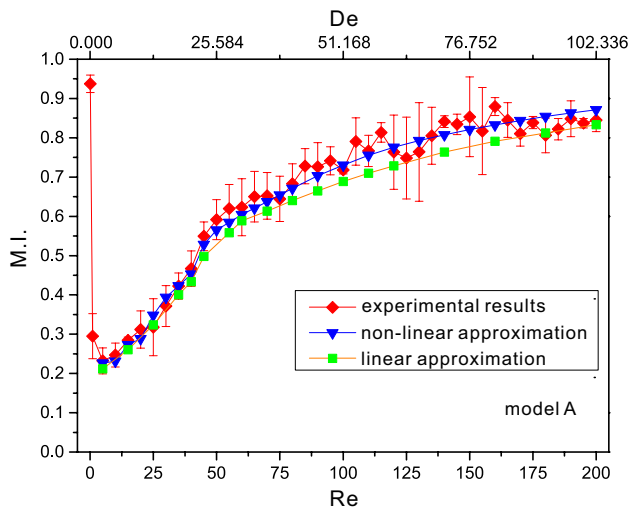


**Fig. 6** Correlation of the mixing index (M.I.) with respect to Reynolds number (Re) and Dean number (De). Nonlinear approximation exhibits a better description of experimental results than linear approximation

viscosity area) from the nonlinear approximation is narrower than that from the linear approximation. Moreover, it is apparent from the displayed distribution nephograms that the linear approximation underrates the diffusion coefficient.

At high flow rate of  $Re = 200$  (Fig. 5b), these differences become significant. The distributions of concentration and viscosity obtained from nonlinear approximation appear to be more uniform, which indicates that the mixing degree is higher than that from the linear approximation. Furthermore, the expansion vortex in the non-coaxial rectangular chamber is more obvious. In contrast, the linear approximation method overestimates viscosity and underestimates diffusion coefficient, both of which change the flow pattern and cause lower mixing efficiency.

Figure 6 shows the comparison between experimental results and numerical results with linear approximation and nonlinear approximation. Dean number of water ( $De = \delta^{0.5}Re$ , where  $\delta$  is the ratio of the channel characteristic length to the flow path radius of curvature and  $Re$  is Reynolds number) is used to evaluate the intensity of secondary flow in the curved channel. The error bars were plotted based on three groups of experimental data. It shows that the results of experiment and simulation with the nonlinear approximation method are in good agreement. Most of the data points locate within the margin of error. A few data points at the outside of error bars (at high flow rate) are mainly caused by the drastic random disturbance. On the contrary, the simulation results of linear approximation show poor accuracy for the reason that the mixing efficiency is lower than the experimental results,

which is consistent with the deduced results based on Fig. 4. At low flow rate of  $Re$  less than 10, viscous effect has a great impact on the flow state. The mixing efficiency depends highly on the effect of molecular diffusion, which is recognized to be a slow process. Thus, the discrepancy between linear and nonlinear approximation is not remarkable. However, this discrepancy becomes apparent as the Reynolds number increases. This phenomenon can be owned to the large viscosity error accumulation of the linear approximation method. Increasing viscosity means reducing  $Re$ . Since  $Re$  describes the relative importance of inertial to viscous forces, the inertial effect is relatively reduced improperly. Consequently, the mixing efficiency is artificially deteriorated. The error of mixing efficiency increases with the viscosity ratio of adopted working fluids. Therefore, the nonlinear approximation shows higher accuracy than the linear approximation.

To further examine the versatility of this nonlinear method and optimize the mixing efficiency, four derived models with different expansion ratios on the non-coaxial rectangular chamber were designed. The mixing process of each model was studied through experiment and modeling by using the nonlinear approximation method. Figure 7 shows variations of the M.I. with  $Re$  ranging from 0.1 to 200. For each model, the results of experiment and simulation are in good agreement and share the similar curve trend. At low flow rate ( $Re < 10$ ), the mixing process is dominated by molecular diffusion. Because extremely low flow rate offers enough residence time for diffusion process, high mixing efficiency is obtained at the condition of  $Re = 0.1$ . However, the M.I. subsequently descends with the increase in  $Re$ , which can be attributed to the reduced residence time. When  $Re$  reaches 15, the mixing efficiency exhibits a slight increase, which indicates that the weak disturbance is induced by the curved channel. As can be seen in Fig. 8, the interfaces among three streams become blur in the curved channel. As the  $Re$  increases further, the secondary flow starts to occur. Under the impact of centrifugal force (Zhang et al. 2015), the fluid close to the inner wall is pulled toward the outer wall and the fluid close to the outer wall is pulled toward the inner wall at the same time. At last, two fluids undergo a  $180^\circ$  rotation and their positions switched. Dean vortices, a pair of vortexes with different directions (clockwise direction and counterclockwise direction, respectively) in the cross section, are intuitively displayed in Fig. 9. The vortexes continuously twist the upper and lower layers of fluid streams, thereby increasing the interfacial area and improving the mixing performance (Yamaguchi et al. 2004). It is observed in Fig. 9 that the intensity of the secondary flow is proportional to the  $Re$ . Hence, the M.I. keeps increasing with the increasing flow rate.

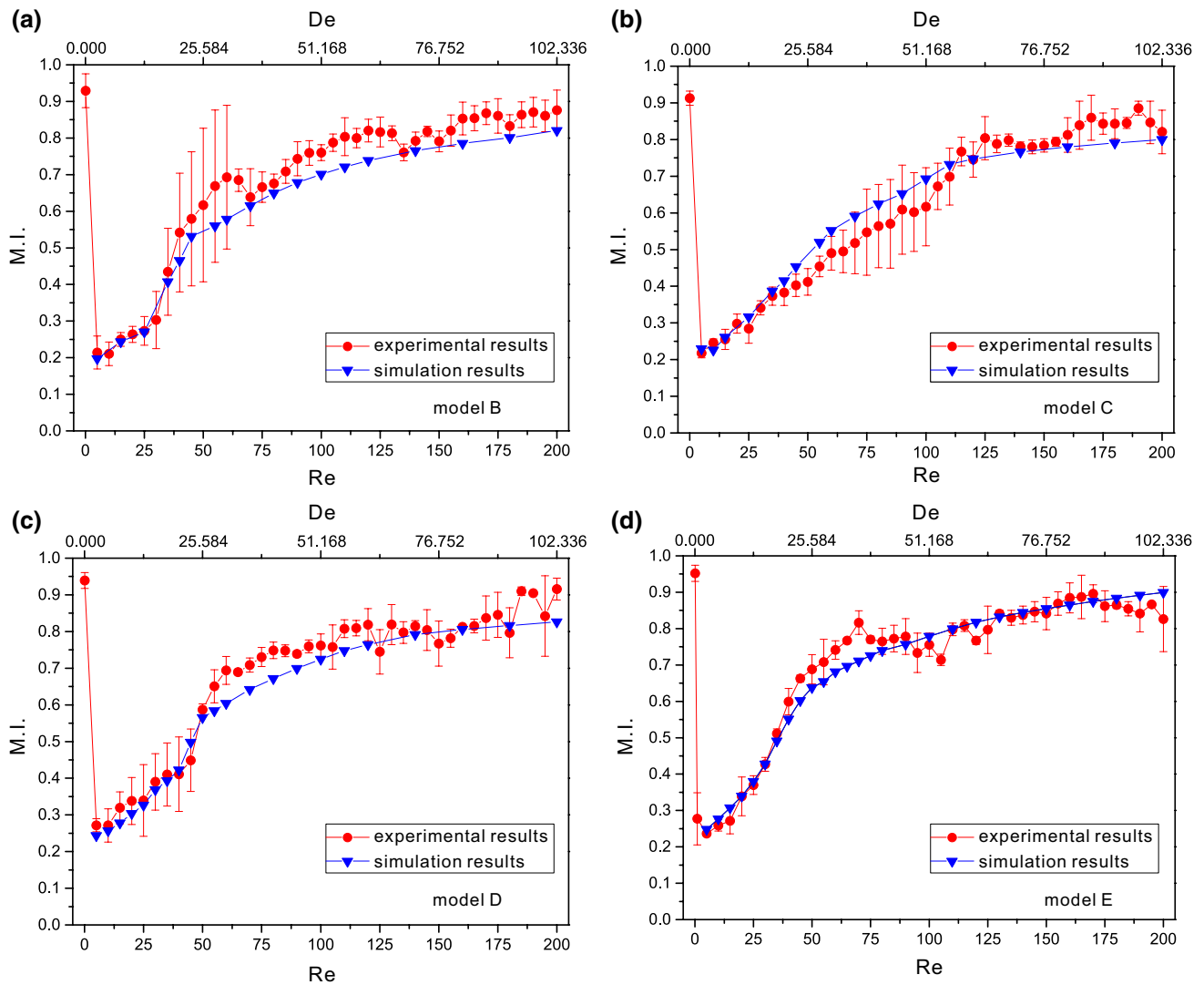


**Fig. 7** Comparison of experimental results and simulation results with respect to the mixing index (M.I.): **a** model B, **b** model C, **c** model D and **d** model E

Until  $Re$  reaches 40, the slope of the curve becomes larger. This can be explained by the appearance of expansion vortex in the expansion chamber (Fig. 8). When flowing into this region at high flow rate, fluids encounter an abrupt expansion in the cross-sectional area. The sudden increase in the cross-sectional area decelerates the fluid flow and separates fluid from the wall due to the inertial effect. This process causes an adverse pressure gradient and reverses the flow; thus, a pair of vortices was formed at each corner of the expansion region (Khodaparast et al. 2014). These multi-direction vortices combine the effect of Dean flow in the curved channel with the effect of expansion vortex in the expansion chamber. Thereby,

these multi-direction vortices accelerate mass transfer and improve the mixing efficiency. In addition, such effects can be reinforced with an increase in flow rate as well. The non-coaxial rectangular chamber comes into play after  $Re$  ascends to a certain value of 50. As shown in Fig. 8, a small circulating flow occurs near the inlet of this chamber. However, the mainstream passes through the chamber without circulating flow since inertial effect is still weak at this time. When  $Re$  gets higher, vortex becomes larger. Under this condition, mainstream is occupied by the vortex. In the presence of circulating flow, the mixing efficiency is further enhanced. Dramatically, the gradient of the M.I. curve becomes small at  $Re > 150$ , which can be ascribed to the

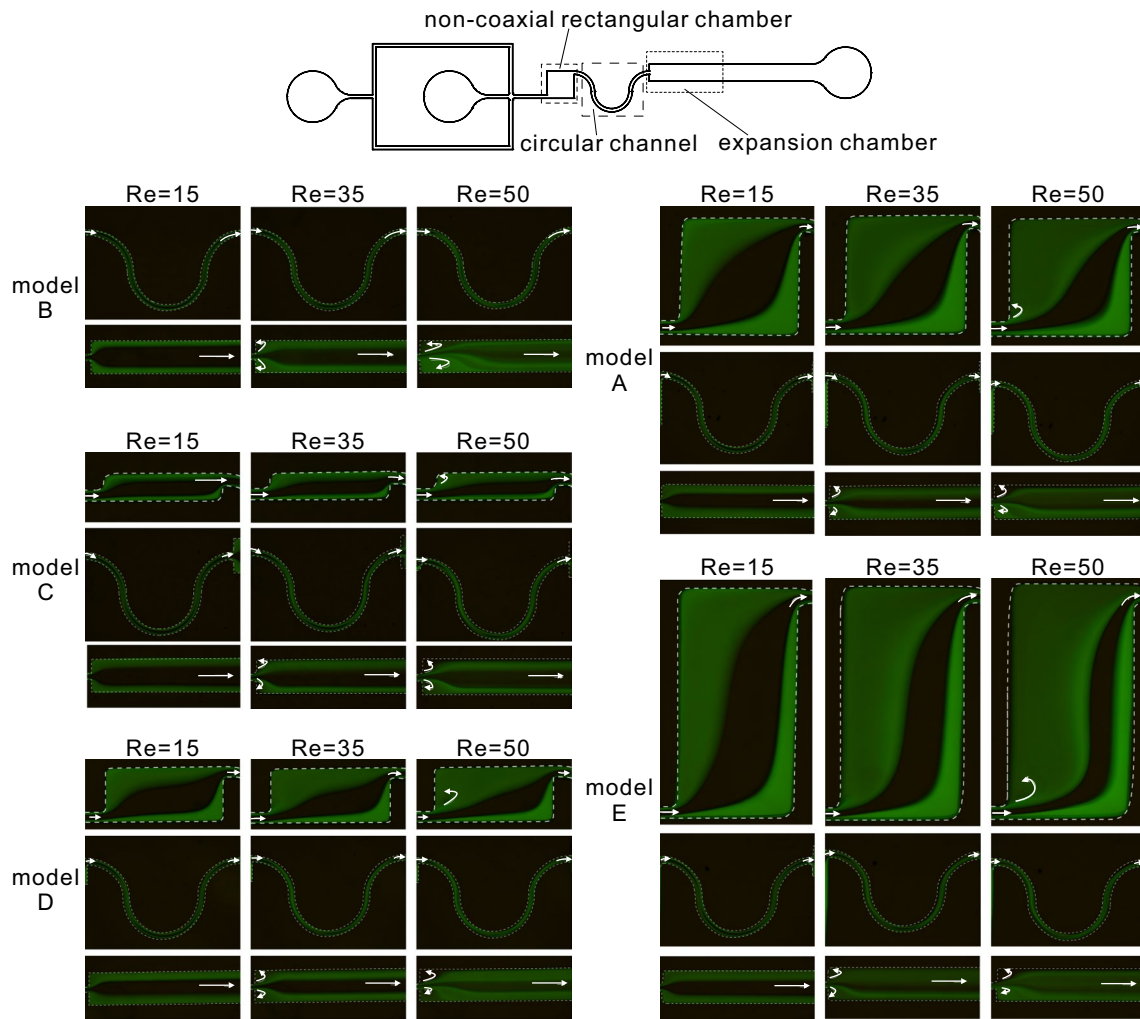


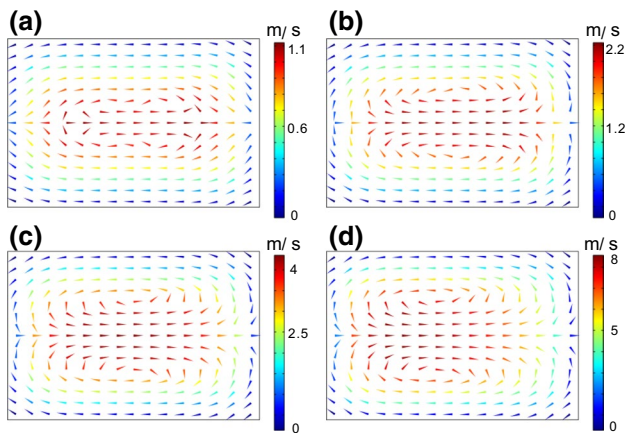
**Fig. 8** Fluid flow distribution of experimental results for model A to model E at different Reynolds numbers (Re) of 15, 35 and 50, respectively. Secondary flow appears in the curved channel for each model at Re = 15. Expansion vortex starts to form in the expansion cham-

ber for each model at Re = 35. With Re = 50, expansion vortex at the location of the non-coaxial rectangular chamber is observed in all models except model B (without this geometry)

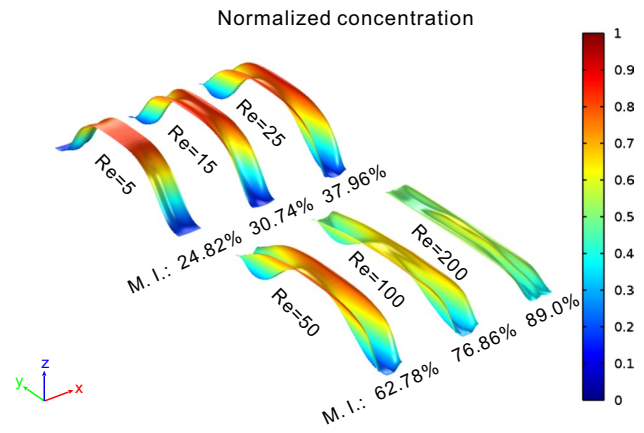
reduced residence time. By this reason, a dynamic equilibrium between disturbance intensity and residence time is established; thus, the highest mixing efficiency is obtained.

Figure 10 depicts the correlations of the mixing index with respect to Reynolds number and Dean number for model A to model E. All of these models give the roughly uniform mixing index at extremely low Re ( $Re = 0.1$ ). The higher mixing efficiency is obtained by model with bigger expansion ratio at  $Re = 10$ . This trend apparently accords with the expansion ratio of each model's non-coaxial rectangular chamber and can be explained by the residence time. It costs more time for fluids to go through the chamber from the model with bigger expansion ratio. At intermediate Re (15–65), M.I. goes up with Re. The ascending gradient of model B is the best in all of the other models

because of pressure loss. Rectangular chamber increases the local pressure loss, but fails to induce strong vortex. Moreover, this loss is also proportional to expansion ratio. For this reason, model B possesses the steepest ascending slope. The M.I. of model B can be distinguished from the other models except model E. The reason is that the non-coaxial rectangular chamber of model E possesses the biggest expansion ratio, which promises enough residence time for molecular diffusion, and this effect exceeds the weak secondary flow in model B at low flow rate. The difference between model E and model B becomes bigger after vortex form in the model E with the increase in Re. At high Re ( $>65$ ), the M.I. of model B is worse than other models because of lacking expansion vortex. As can be seen in Fig. 11, the deformation of the pseudo-color image



**Fig. 9** Evolution of secondary flow at the cross section of A–A with: **a**  $Re = 25$ , **b**  $Re = 50$ , **c**  $Re = 100$  and **d**  $Re = 200$ . The intensity of the secondary flow is directly proportional to Reynolds number ( $Re$ )



**Fig. 11** Distributions of normalized concentration at the outlet of model E with different Reynolds numbers ( $Re$ ) of 5, 15, 25, 50, 100 and 200. The *vertical axis* represents the normalized concentration. When  $Re > 5$ , mixing index (M.I.) increases with the increase in Reynolds number ( $Re$ )

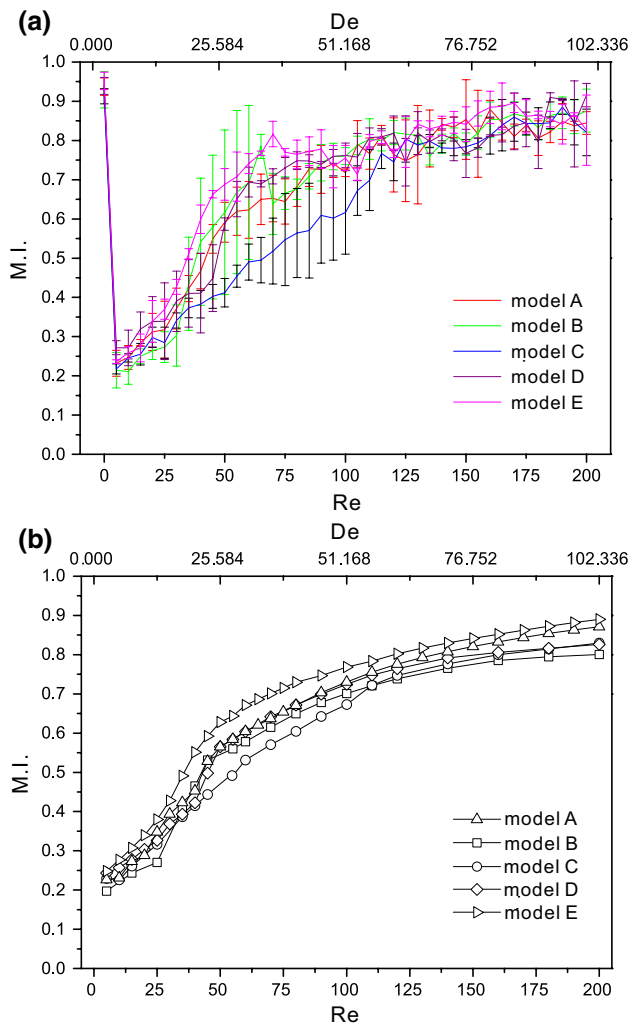


**Fig. 10** Correlations of the mixing index (M.I.) with respect to Reynolds number ( $Re$ ) and Dean number ( $De$ ) for model A to model E based on: **a** experimental results and **b** simulation results

gradually tends to flatten out for  $Re$  from 5 to 200, which means the concentration distribution becomes uniform with the increase in flow rate.

### 5 Summary

In this work, a group of coupling relationships in terms of fluid properties such as density, viscosity, and diffusion coefficient were introduced into the numerical models to simulate the mixing process of glycerol solution and water. With the application of these relationships, viscosity and diffusion coefficient are turned into concentration dependent and determined by the local concentration in the micro-channel. A preliminary theoretical comparison between the traditional linear approximation and the nonlinear method has been carried out. To validate the nonlinear method, modeling and experiment techniques were performed on a novel micromixer. The comparison shows that the nonlinear approach achieves higher accuracy and is more suitable to simulate the viscous mixing than the linear approximation. Furthermore, to examine the versatility of this nonlinear method, four derived models were designed and tested. The experimental results and numerical results are in good agreement for each model. To sum up, accounting for the effect of ever-changing viscosity, the modeling with nonlinear couplings exhibits a better description of experimental results than linear approximation.

**Acknowledgments** The authors would like to thank the fellows involved in this work for their fervent assistance and useful advices. ZG Wu thanks the Hubei Natural Science Foundation (Contract No. 2015CFA110) and Chinese central government via its Recruitment Program for Innovative Talents (youth group) for the financial support.

## References

- Alam A, Afzal A, Kim KY (2014) Mixing performance of a planar micromixer with circular obstructions in a curved microchannel. *Chem Eng Res Des* 92:423–434
- Ansari MA, Kim KY (2009) A numerical study of mixing in a microchannel with circular mixing chambers. *AIChE J* 55:2217–2225
- Auroux PA, Iossifidis D, Reyes DR, Manz A (2002) Micro total analysis systems. 2. Analytical standard operations and applications. *Anal Chem* 74:2637–2652
- Cheng NS (2008) Formula for the viscosity of a glycerol-water mixture. *Ind Eng Chem Res* 47:3285–3288
- Cheri MS, Latifi H, Moghaddam MS, Shahraki H (2013) Simulation and experimental investigation of planar micromixers with short-mixing-length. *Chem Eng J* 234:247–255
- Cook KJ, Fan YF, Hassan I (2013) Mixing evaluation of a passive scaled-up serpentine micromixer with slanted grooves. *J Fluid Eng* 135:14–16
- Hessel V, Löwe H, Schönfeld F (2005) Micromixers—a review on passive and active mixing principles. *Chem Eng Sci* 60:2479–2501
- Jeong GS, Chung S, Kim CB, Lee SH (2010) Applications of micromixing technology. *Analyst* 135:460–473
- Khodaparast S, Borhani N, Thome JR (2014) Sudden expansions in circular microchannels: flow dynamics and pressure drop. *Microfluid Nanofluid* 17:561–572
- Kuo JN, Jiang LR (2014) Design optimization of micromixer with square-wave microchannel on compact disk microfluidic platform. *Microsyst Technol* 20:91–99
- Lee CY, Wang WT, Liu CC, Fu LM (2016) Passive mixers in microfluidic systems: a review. *Chem Eng J* 288:146–160
- Nguyen NT, Wu ZG (2005) Micromixers—a review. *J Micromech Microeng* 15:R1–R16
- Patabadige DEW, Shu J, Sibbitts J, Sadeghi J, Sellens K, Culbertson CT (2016) Micro total analysis systems: fundamental advances and applications. *Anal Chem* 88:320–338
- Reyes DR, Iossifidis D, Auroux PA, Manz A (2002) Micro total analysis systems. 1. Introduction, theory, and technology. *Anal Chem* 74:2623–2636
- Sackmann EK, Fulton AL, Beebe DJ (2014) The present and future role of microfluidics in biomedical research. *Nature* 507:181–189
- Solehati N, Bae J, Sasmito AP (2014) Numerical investigation of mixing performance in microchannel T-junction with wavy structure. *Comput Fluids* 96:10–19
- Sudarsan AP, Uguz VM (2006) Fluid mixing in planar spiral microchannels. *Lab Chip* 6:74–82
- Ward K, Fan ZH (2015) Mixing in microfluidic devices and enhancement methods. *J Micromech Microeng* 25(9):094001
- Wu Z, Nguyen NT (2005) Hydrodynamic focusing in microchannels under consideration of diffusive dispersion: theories and experiments. *Sensors Actuators B Chem* 107:965–974
- Wu CY, Tsai RT (2013) Fluid mixing via multidirectional vortices in converging–diverging meandering microchannels with semi-elliptical side walls. *Chem Eng J* 217:320–328
- Wu Z, Nguyen NT, Huang X (2004) Nonlinear diffusive mixing in microchannels: theory and experiments. *J Micromech Microeng* 14:604–611
- Xia Y, Whitesides GM (1998) Soft Lithography. *Angew Chem Int Ed* 37:550–575
- Yamaguchi Y, Takagi F, Watari T, Yamashita K, Nakamura H, Shimizu H, Maeda H (2004) Interface configuration of the two layered laminar flow in a curved microchannel. *Chem Eng J* 101:367–372
- Zhang J, Yan S, Yuan D, Alici G, Nguyen NT, Warkiani ME, Li W (2015) Fundamentals and applications of inertial microfluidics: a review. *J Math Anal Appl* 50:273–287